

Fluid Flow Distribution and Pressure Drop in Split P Lattice TPMS Structures with Varying Wall Thickness

S.U Zainal^{1, 2}, Yupiter HP Manurung^{1, 2}, Mohd Shahrman Adenan^{1*, 2},
Mohd Faizal Mohamad^{1, 2, 3}, Wan Ahmad Najmi Wan Mohamed^{2, 4}

¹Smart Manufacturing Research Institute, Universiti Teknologi MARA, 40450, Shah Alam, Selangor, Malaysia

²Faculty of Mechanical Engineering, Universiti Teknologi MARA, 40450, Shah Alam, Selangor, Malaysia

³Wind Engineering & Building Physics, Universiti Teknologi MARA, 40450, Shah Alam, Selangor, Malaysia

⁴Efficient Energy Conversion Technologies Research Group, Universiti Teknologi MARA, 40450, Shah Alam, Selangor, Malaysia

ARTICLE INFO

Article history:

Received 22 October 2024

Revised 14 March 2025

Accepted 19 March 2025

Online first

Published 15 May 2025

Keywords:

Direct air capture

Carbon capture

Triply periodic minimal surface (TPMS)

Computational fluid dynamics (CFD)

Split P lattice

DOI:

<https://doi.org/10.24191/jmeche.v22i2.3709>

ABSTRACT

Design for additive manufacturing (DfAM) has enabled the creation of complex lattice structures using selective laser melting (SLM) in additive manufacturing (AM). This study focuses on triply periodic minimal surfaces (TPMS), specifically the split P lattice, which optimizes fluid flow in gas-solid contacting systems for carbon capture applications. The TPMS design enhances gas interaction with large surface areas, crucial for improving mass transfer in chemical processes. Despite significant research on TPMS structures, comprehensive fluid flow analysis for split P lattices in direct air capture (DAC) systems remains limited. This study investigates the effects of varying wall thicknesses (0.4 mm, 0.8 mm, and 1.2 mm) under laminar flow conditions in 5 mm unit cells, across Reynolds numbers (Re) ranging from 25 to 125. Results show that the TPMS structure increases the surface area by 35% and boosts inlet velocity up to fourfold. Thicker walls lead to higher pressure drops and localized acceleration, resulting in a higher velocity profile within smaller pores. The 0.8 mm wall thickness demonstrated the best balance, offering superior area-averaged velocity and uniform flow distribution. Compared to previous TPMS studies, the split P lattice design achieves a more uniform distribution and improved permeability, making it a promising solution for DAC reactor performance.

INTRODUCTION

Design for additive manufacturing (DfAM) is a methodology aimed at optimizing functional performance by leveraging the unique capabilities of additive manufacturing (AM) technologies. AM enables the

^{1*} Corresponding author. E-mail address: mshahrman@uitm.edu.my
<https://doi.org/10.24191/jmeche.v22i2.3709>

production of highly complex structures through a layer-by-layer material deposition process (Plocher & Panesar, 2019). Unlike subtractive manufacturing, where material is removed from a solid block to form the final product, AM offers the flexibility to create intricate geometries with minimal waste. This technological advancement has transformed sectors such as aerospace, healthcare, and chemical engineering by enabling the development of lightweight, high-performance components with optimized material usage and enhanced functionality (Xu et al., 2021; Zhang et al., 2021).

The American Society for Testing and Materials (ASTM) established the "ASTM F42 – Additive Manufacturing" group, which defines standards for classifying AM processes into seven categories including vat photopolymerization, material jetting, binder jetting, material extrusion, powder bed fusion (PBF), sheet lamination, and directed energy deposition. Among these, PBF has proven particularly effective for fabricating functional parts from metals and alloys. PBF encompasses several techniques, including direct metal laser sintering (DMLS), electron beam melting (EBM), selective heat sintering (SHS), selective laser melting (SLM), and selective laser sintering (SLS) (Kawalkar et al., 2022). SLM stands out due to its ability to achieve higher part densities compared to other PBF methods, where the high energy density of laser beam promotes full material fusion and eliminates porosity (Nagarajan et al., 2019). SLM has gained broad industrial adoption due to its capability to directly manufacture fully dense metal components without binders or additional processing (Rabuan et al., 2023; Maconachie et al., 2019). The process involves spreading a thin layer of metal powder over a build platform and selectively melting it using a laser beam and controlled by a galvanometer, to fuse specific regions. This process, repeated layer by layer, is ideal for producing complex geometries such as lattice structures, which are critical for optimizing performance in various applications.

The concept of 3D design in engineering frequently utilizes lattice structures, which are repeating patterns that fill a volume or space. These lattices, inspired by natural forms, include beams, plates, honeycombs, triply periodic minimal surfaces (TPMS), and stochastic lattices, each offering distinct structural benefits for various applications (Maskery et al., 2018; Yin et al., 2021). Lattices are particularly valued for their ability to meet lightweight design requirements while maintaining mechanical strength. TPMS, which is mathematically defined, surfaces with intricate, repeating topologies, and divides space into interconnected domains. Stainless steel TPMS structures fabricated using SLM have been reported to exhibit exceptional properties such as high surface density, permeability, functional gradability, and optimal thermal conductivity (Laskowska et al., 2023). The geometry of TPMS lattices significantly affects fluid flow, impacting parameters such as velocity, pressure drop, permeability, and mixing (Hawken et al., 2023; Li & Iskander, 2022). In single-phase flow through a lattice medium, four flow regimes are recognized, which are creeping (Darcy or Stokes flow), inertial (steady laminar), transitional (unsteady laminar), and turbulent flow (Wood et al., 2020). These transitions are governed by the Reynolds number (Re) to determine the relative importance of inertia and viscous effects.

Various types of TPMS lattices, including gyroid, diamond, split P, primitive, lidinoid and neovious have been explored for their unique structural properties across multiple engineering fields such as tissue engineering, structural engineering, phase change cooling, and heat transfer. Notably, TPMS lattices are gaining attention due to their potential to optimize both mechanical and thermal performance. For instance, studies on TPMS-based heat sinks have demonstrated that diamond structures, under forced convection heat transfer, outperform gyroid structures, achieving a 32% improvement in thermal performance under similar flow conditions (Al-Ketan et al., 2020). Additionally, research on heat exchangers revealed that the primitive TPMS structure concentrates high-velocity fluid flow near the central region of the cross-section, while the lidinoid structure exhibits the highest local acceleration, with velocities 2.3 times greater than those in the lidinoid structure (Xu et al., 2023; Xu et al., 2023). Although most studies on the split P structure focus on its energy absorption properties, such as its high specific stiffness and energy dissipation due to its large surface area, there is significant potential for further investigation into its fluid flow characteristics (Miralbes et al., 2022). The split P morphology marked by large pore size, a high surface area-to-volume

ratio, and pronounced local curvature suggests promising applications in optimizing fluid dynamics and enhancing mass transfer processes.

Agendas 7 and 13 of the Sustainable Development Goals emphasize the urgent need for active carbon mitigation strategies, with a key focus on reducing carbon dioxide (CO₂) emissions. Direct air capture (DAC) systems designed to remove CO₂ from ambient air rely heavily on adsorption bed configurations to increase surface area for gas-solid contact. However, current large bed designs face significant challenges in optimizing CO₂ capture efficiency due to non-uniform mass and heat transfer rates. These inefficiencies disrupt the adsorption equilibrium and limit the reactor's overall performance. While conventional packed bed reactors can enhance contact area through structured or random packing, such as Raschig rings (Alix et al., 2019). The design faces a problem with high flow rates, often leading to increased energy consumption and diminished adsorption capacity (Gunawardene et al., 2022). Achieving uniform flow distribution and effective heat and mass transfer within these systems remains a major challenge in DAC technology. A promising solution to these limitations is the use of structured packing designs such as the split P lattice configuration, which offers better control over gas-solid interactions. The split P design maximizes surface area while lowering resistance, enabling more efficient airflow through the reactor and enhancing CO₂ contact between the sorbent materials. This could lead to faster adsorption kinetics and improved mass transfer (Baghapour et al., 2018; Young et al., 2023). Additionally, the structured reactor flow characteristics allow for higher flow rates and more complete saturation of the sorbent bed, significantly improving adsorption efficiency compared to traditional fixed bed designs (Dhoke et al., 2021; Zimmer et al., 2021). This structured approach has the potential to increase adsorption rates by 3 to 10 times, making it a key innovation in optimizing DAC reactor performance.

Recent research on reactor design for carbon capture focuses on optimizing key operating parameters such as adsorption time, gas velocities, contact efficiency, and gas-solid interactions (Yu & Brilman, 2017). The advent of additive manufacturing has enabled the creation of intricate 3D structured packings, specifically designed to enhance mass transfer performance in adsorption systems (Ellebracht et al., 2023). This study investigates the design and performance of split P lattice structures for DAC applications, employing computational fluid dynamics (CFD) analysis. Despite extensive studies on TPMS-based structures, a research gap exists regarding the specific influence of split P lattice geometries on flow performance in carbon capture applications as a base exploration for future thermal and carbon adsorption assessments. This study addresses the limitation by evaluating the effect of varying wall thickness on the velocity profile and pressure drop within split P lattice structures. By investigating these parameters, this research provides insights into optimizing TPMS designs for carbon capture applications. The analysis focuses on critical factors influencing CO₂ adsorption kinetics, specifically the fluid-surface interactions, velocity, and pressure profiles. By examining the effects of the split P configuration on these parameters, this study offers valuable insights into improving DAC reactor efficiency and contributes towards future advancements in structured lattice designs for carbon capture systems.

METHODOLOGY AND RESEARCH MATERIAL

Design of Split P Lattice

The level set equation for the split P structure is derived using the Cartesian coordinate system (X , Y , Z) and a specified isovalue. This isovalue is commonly used in mathematical and computational modeling to define a surface in 3D space, particularly in level set methods or implicit surface modeling. The isovalue directly influences the design and characteristics of the lattice structure. The mathematical expression of the split P structure in Equation 1 (Lehder et al., 2021).

$$1.1((\sin 2X \cos Y \sin Z) + (\sin 2Y \cos Z \sin X) + (\sin 2Z \cos X \sin Y)) - 0.2 ((\cos 2X \cos 2Y) + (\cos 2Y \cos 2Z + (\cos 2Z \cos 2X))) - 0.4 (\cos 2Y + \cos 2X + \cos 2Z) - t = \varphi \quad (1)$$

where $X, Y, Z = 2\pi \frac{\eta_i}{L_i}$, $i = x, y, z$ represents the periodicities of the split P structure, the variable η_i denotes the number of unit cell along x, y, z direction while L_i indicates the unit cell in each respective direction. Reducing the wavelength results in smaller cells, increasing the surface-to-volume ratio but decreasing bed porosity, which ultimately leads to higher flow resistance. This study generates split P lattice structures using nTop (version 4.2.2), a software capable of creating cubical triply periodic minimal surfaces (TPMS) structures. The DAC domain was scaled down to $10 \times 10 \times 10$ mm for simulation purposes, particularly to improve mesh resolution and preliminary design evaluation. To investigate the impact of design parameters of the split P lattice, the wall thickness was varied at 0.4 mm (SP0.4), 0.8 mm (SP0.8), and 1.2 mm (SP1.2). Illustrates the domain and split P lattice structures with different wall thicknesses (see Fig 1), and the specifications of each design variation (Table 1).

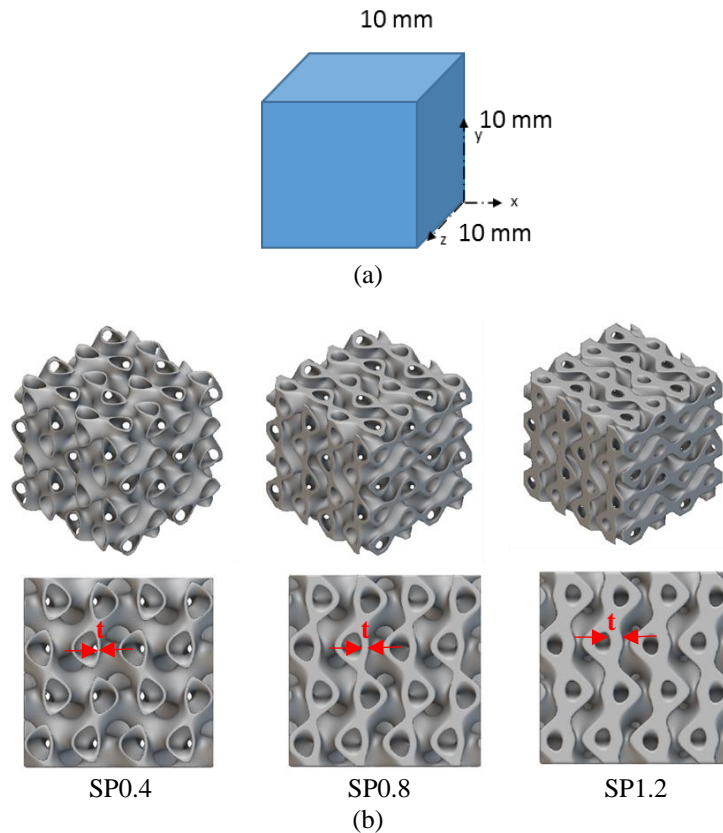


Fig. 1. Comparative design configuration for split P lattice (a) a baseline cubic unit cell, and (b) TPMS split P lattice structures with variable in-wall thickness, t .

Porosity

Porosity percentage represents the void space within the material and is calculated as in Equation 2. Porosity, denoted by ε , is defined as the volume of total V_T and solid V_S material. SP0.4 exhibits the highest porosity at 80%, followed by SP0.8 and SP1.2, with porosities of 58% and 38%, respectively (Table 1). Structures with higher porosity promote more efficient fluid diffusion and transport through the material (Patil et al., 2022).

$$\varepsilon = 1 - \left(\frac{V_s}{V_T} \right) \times 100 \quad (2)$$

Table 1. Properties of TPMS split P lattice structures with varying wall thicknesses

Split P model	Unit cell (mm)	Thickness, t (mm)	Volume (mm ³)	Surface area (mm ²)	Mass (g)	Porosity (%)
SP0.4	5	0.40	209.64	2128.55	1.68	80
SP0.8	5	0.80	420.68	2111.92	3.37	58
SP1.2	5	1.20	624.42	1919.91	5.00	38

Design Configuration and Boundary Conditions

The STL file generated from nTop was exported to OpenFoam for computational fluid analysis. Generic meshing libraries, such as blockMesh (BM) for the background mesh and SnappyHexMesh (SHM), were employed to create separate volume meshes for the solid and fluid regions. A mesh sensitivity analysis was specifically performed using a total of 6.4×10^5 cells to define the domain. The closed channel within the simulation domain has dimensions of $70 \times 10 \times 10$ mm (see Fig 2). Air enters through the inlet, flows through the channel, and exits through the outlet. The split P lattice domain is located at the middle point of the channel, with the centre line of the lattice positioned 0.035 m from both the inlet and outlet. The channel walls and TPMS surfaces are both assigned appropriate wall boundary conditions. Laminar inlet velocities of 0.03 ms^{-1} , 0.07 ms^{-1} , 0.10 ms^{-1} , 0.13 ms^{-1} , and 0.17 ms^{-1} were set to achieve Reynolds 25, 50, 75, 100, and 125, respectively, for simulation cases, allowing for different flow scenarios in DAC (Table 2) (Attarzadeh et al., 2021).

Table 2. Applied boundary conditions for simulations

Inlet	Re numbers	U (m/s)	$v = w = 0$
	25	0.03	
	50	0.07	
	75	0.10	
	100	0.13	
	125	0.17	
Outlet	$\frac{\partial u_{inlet}}{\partial x} = \frac{\partial T}{\partial x} = 0$		
Left and right	$\frac{\partial u}{\partial z} = \frac{\partial v}{\partial z} = 0$		$w = 0$
Top and bottom	$\frac{\partial u}{\partial y} = \frac{\partial v}{\partial y} = 0$		$v = 0$

Mathematical Model

The simulation employed the finite volume method (FVM) for equation discretization and implemented the SIMPLE algorithm. This study simulated fluid flow through a channel containing 3D lattice packings under laminar flow conditions at different inlet velocities. The governing equations used were the

momentum and continuity equations for incompressible flow using Equations 3 and 4, respectively (Jiang et al., 2023; Bragin et al., 2024).

$$\frac{\partial \vec{u}}{\partial t} + \nabla(\vec{u}\vec{u}) = -\nabla p + \nu \nabla(\nabla \vec{u}) \quad (3)$$

$$\nabla \cdot \vec{u} = 0 \quad (4)$$

In this equation, \vec{u} denotes the velocity vector, p is the kinematic pressure, and ν is the kinematic viscosity. The inlet velocity was calculated using Equation 5 of the Reynolds for every case (Xu et al., 2023).

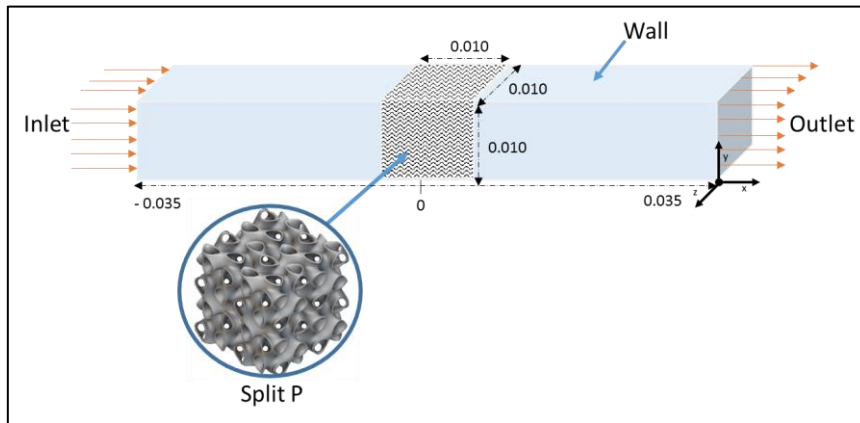


Fig. 2. Arrangement of the computational domain and boundary conditions.

$$Re = \frac{\rho D U}{\mu} \quad (5)$$

where U is the inlet velocity, D is the hydraulic diameter for a square duct, ρ refers to air density, approximately at $1.204 \frac{kg}{m^3}$, and μ is the air viscosity of $1.60 \times 10^{-5} \frac{m^2}{s}$. Darcy's law states that in a porous media, the pressure drop per unit length is directly proportional to the fluid velocity in laminar flow in Equation 6 (Karaman & Asl, 2023),

$$\frac{\Delta p}{\Delta L} = \frac{\mu}{K} \cdot U \quad (6)$$

where Δp is the pressure differential along the channel, ΔL is the length of the channel, and K is the permeability of the porous media.

RESULTS AND DISCUSSION

Analysis Focus and Limitations

For DAC application, it is desirable to have an active fluid-surface interaction for the carbon desorption mass transfer reaction to occur. The geometry of the split P design is similar, but the pore sizes are different due to the variation in the wall thickness. As porosity decreases, the pore area becomes smaller and local flow resistance increases, inducing a variation of pressure gradient within the internal pores, resulting in higher velocity separation within the lattice. This potentially leads to the generation of vortices that can reduce contact time between the sorbent and the wall (Gado et al., 2023; Chen et al., 2024; Tang et al., 2023). Therefore, a specific split P design must be identified that balances the requirement for uniform flow distribution, flow strength (local velocity), flow conditions (vortices), and pressure distribution (local partial pressure) for a carbon adsorption DAC application. The evaluation in this current study is limited to the flow distribution and optimization of the split P design, influenced by the initial flow strength (inlet Reynolds number). The results indicate active fluid-surface interaction within the lattices along the flow direction.

Regions with low velocities (approaching 0 m/s) are considered non-reactive for carbon adsorption purposes. Flow distribution profiles with high velocities, especially at the surfaces of the lattice, are the profiles required and best suited for DAC application, as they indicate rapid and active fluid-surface interaction.

Flow Stream Along the Channel

An example of the velocity profile along the flow channel with respect to xy and xz planes (see Fig 3) for inlet $Re = 75$. For all split P models, an increase in velocity was observed in the middle of the plane due to the development of fully developed flow. It is evident that the air flow velocity is higher in the center compared to the velocity at the channel walls due to surface friction. Consequently, the flow entering the split P cells has a non-uniform flow where a fully developed flow is assumed. The maximum velocity is in the center of the fluid stream and approaches zero at the channel wall surfaces. Thus, the presented analysis on the fluid flow within the split P lattices is based on the fully developed inlet flow stream. This has provided an overview of the effect of the split P lattices on the flow stream. An increase in fluid velocity is evident as it exits the cell due to the pressure reduction effect within the pores. Generally, the exit velocity is higher for SP1.2 due to the smaller pore sizes, and its flow strength is sufficient to maintain a consistent streamline towards the exit of the channel, whereas a certain degree of backpressure effect can be expected for the SP0.4 and SP0.8 designs due to the lower exit flow strength. However, the backpressure effect takes place further downstream and does not influence the flow stream profile within the split P cells.

Velocity Distribution in TPMS Split P Cells

Visualization of the flow separation zone is based on the five planes along the split P lattice (see Fig 4). The planes are at positions a , b , c , d , and e , at distances of -0.5 mm, -0.3 mm, 0.0 mm (split P mid-point), 0.3 mm, and 0.5 mm, respectively, positioned along the x -axis of the split P cell. The lattice surfaces are modelled with zero mean curvature, therefore enabling unhindered flow in all directions as the fluid enters the lattice geometry (Peng et al., 2020). The generation of a spinning helical flow motion within the lattices due to the rapid changes in local Reynolds number, influenced by local pressure gradients (see Fig 5). This helical motion occurs at the center of the unit cell and is the key mechanism towards improving fluid-surface interactions.

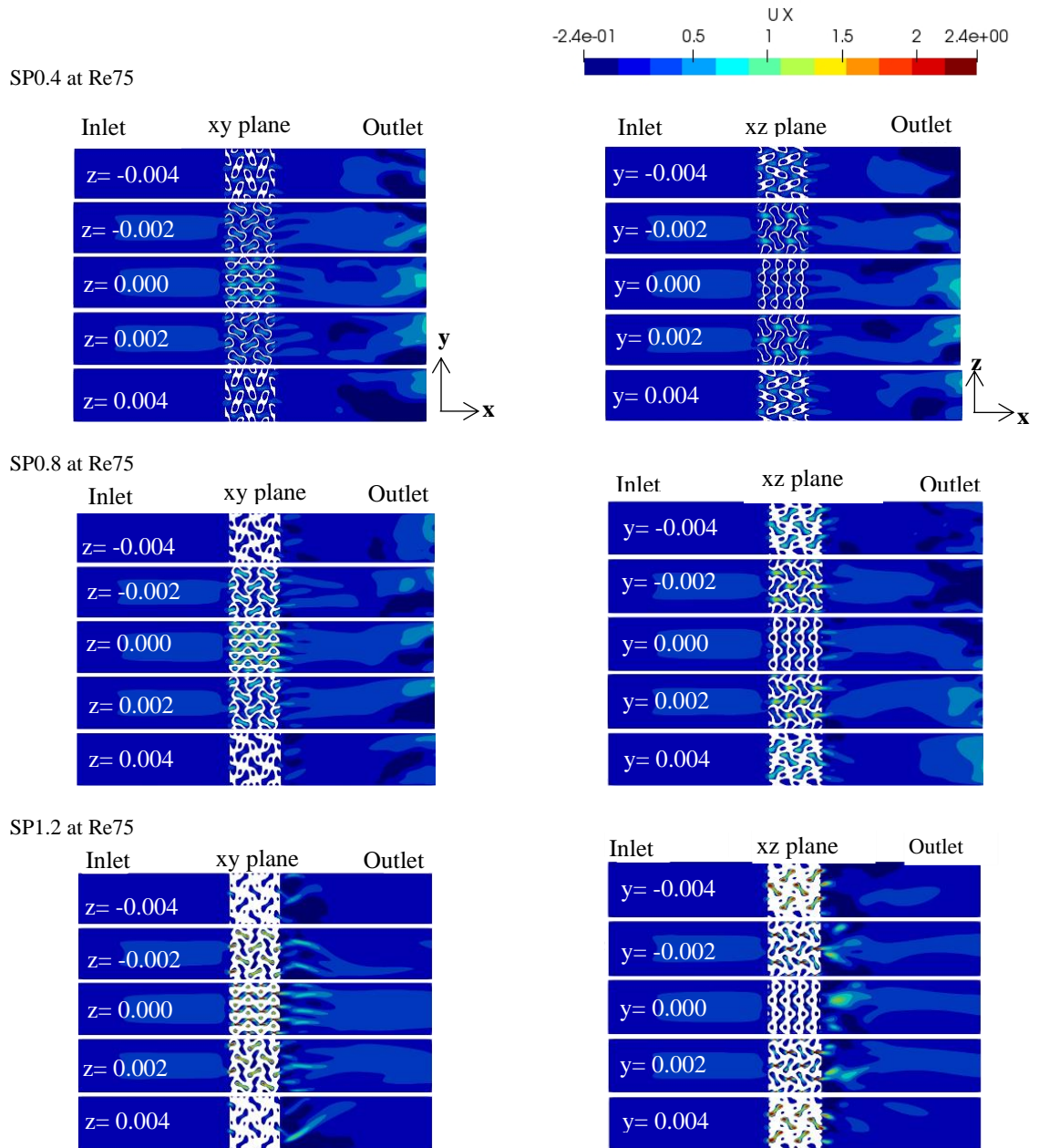


Fig. 3. Comparative fluid flow profiles within split P lattice structures (SP0.4, SP0.8, and SP1.2) based on the fully developed initial flow stream at Re75 visualized in the xy and xz planes.

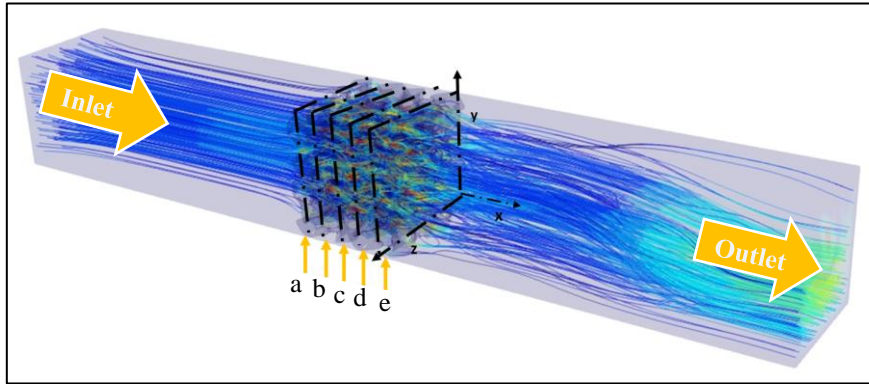


Fig. 4. Velocity streamlines and dispersion within SP0.4 at $Re=100$. Cross-sections on the yz plane at a , -0.5 mm; b , -0.3 mm; c , 0.0 mm; d , 0.3 mm, and e , 0.5 mm.

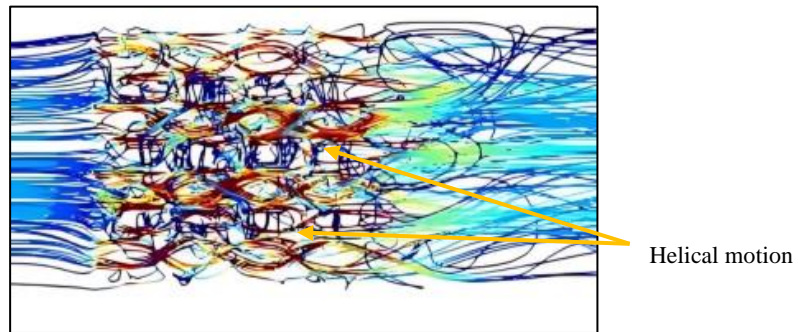
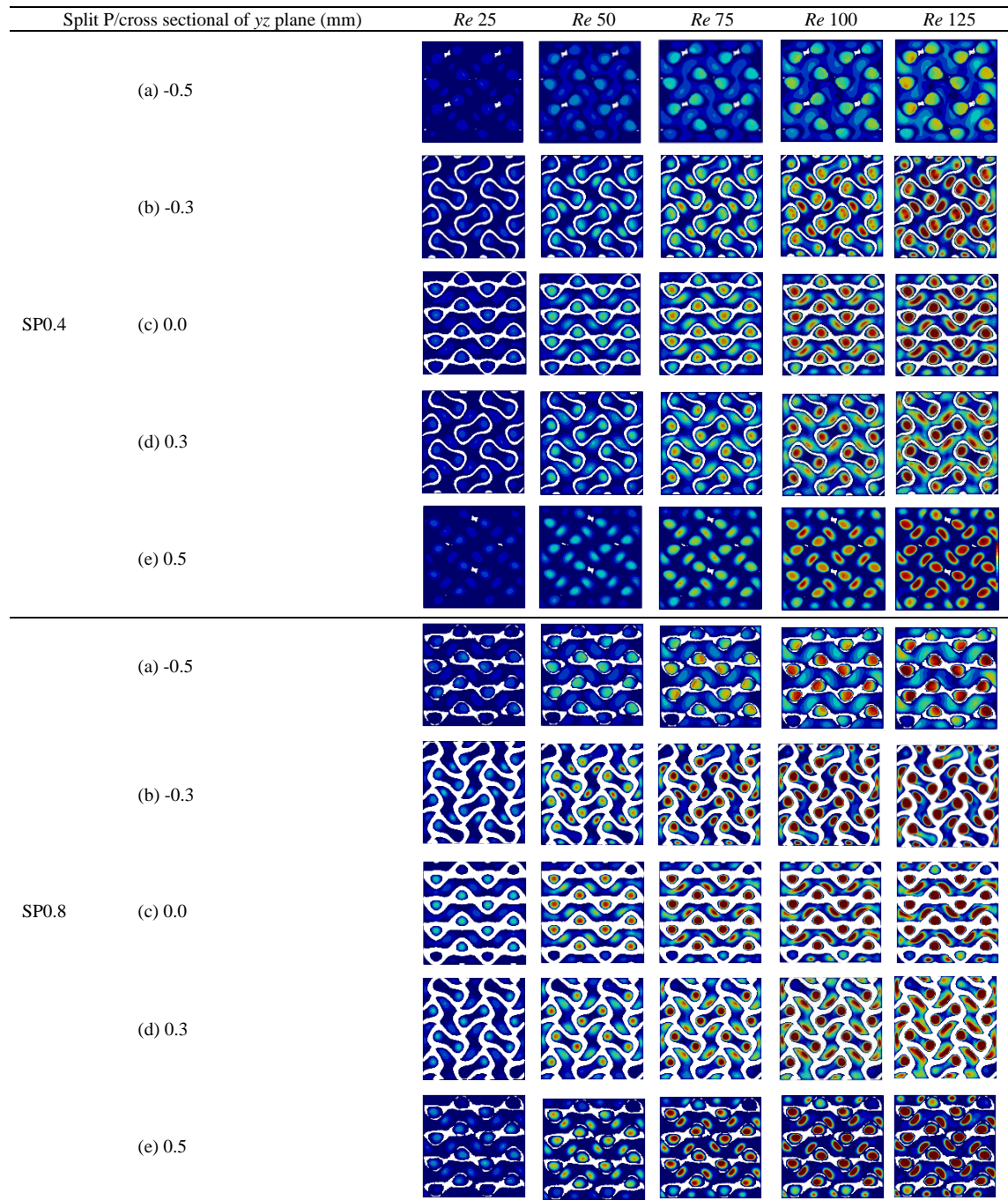


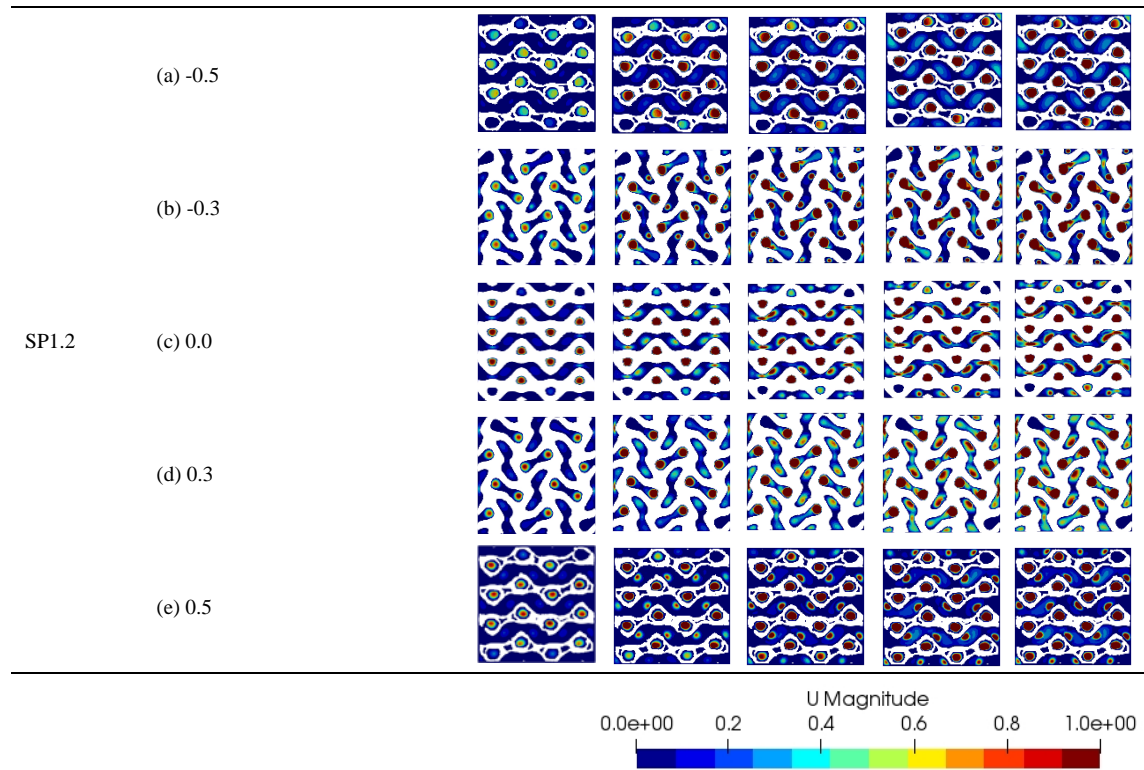
Fig. 5. Visualization of helical motion patterns leading to enhanced mixing and velocity flow within the internal geometry.

The flow pattern along the five planes under different split P designs and inlet Reynolds number (see Table 3). The flow transition is generally eccentric due to directional changes in the helical motion, influenced by the individual split P designs. As an overview, the flow velocities are low at positions a and b compared to flow velocities at positions c , d , and e because of pressure reduction along the cell. The size of the split P pores indicates pressure reduction and the relative local velocities, thereby influencing the overall flow distribution and fluid-surface interaction. The SP0.4 design clearly fails to induce an effective fluid-surface interaction at low inlet Reynolds numbers of 25 and 50, as there are large zones with near-zero velocities. The initial flow strength is too low to generate a significant increase in velocity and uniform distribution within the lattice cell. The effect is only significant when the inlet Reynolds number is higher than 75, as higher velocities are induced, and the fluid covers a greater area of the lattice cell. A high inlet Reynolds number (greater than 75) is needed to obtain a more uniform flow distribution and significant fluid-surface interaction for the SP0.4 design. The SP0.8 design is more adaptive to low inlet Reynolds numbers. Visible velocity increase is obtained at $Re = 50$, but the fluid-surface interaction is considered good for DAC application only at an inlet Reynolds number of 75 and higher. The SP01.2 design with the smallest pore size displays the best velocity increase, flow distribution, and fluid-surface interaction. It is suitable even for low inlet Reynolds numbers and demonstrates a strong capability to increase flow velocity, ensuring a more uniform distribution within the lattice cells (D'Orazio et al., 2023). The fluid is allowed to fully occupy the cell zones as the velocity contour at $Re = 125$ shows very minimal zones with near zero

fluid velocity. It would provide the required conditions for the optimal carbon adsorption process to occur due to the active contact of the fluid with the lattice surfaces.

Table 3. Velocity distribution within TPMS split P lattice structures viewed from the yz plane





However, the surface area of SP1.2 for carbon adsorption is lower than SP0.8 due to the higher wall thickness. Therefore, SP0.8 is better suited for DAC application as it provides a balance between the total adsorption surface area and fluid-surface interaction area. The exact interaction ratio is not presented in this manuscript as it requires a further image processing algorithm to obtain the required values.

Velocity Profile Inside the Channel

The area-averaged fluid velocity at the designated yz plane (see Fig 6). A lattice structure evidently increases the flow velocity as the fluid flows through the central region ($y, z = 0, 0$) of the cross section along the direction of the channel (x -axis). This is because, in this region, the velocity has reached its maximum velocity due to the fully developed flow in the channel. The impact of wall thickness is also evident where pores with greater sizes register greater area-averaged velocity due to lower pressure reductions (see Fig 7). The streamwise velocity magnitude in the x -direction is increased by an average of 125% for SP0.8, while the increments are only 96% and 82% for SP0.4 and SP1.2, respectively. The high average velocity is due to reduced resistance to flow, which allows a greater amount of fluid to pass through.

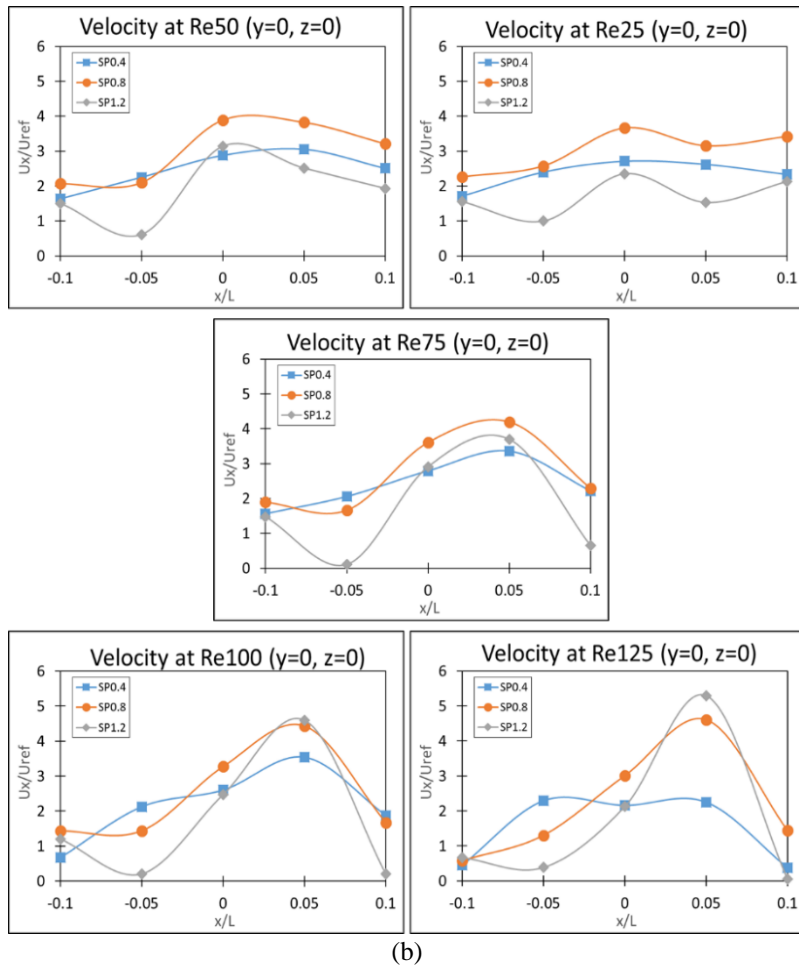
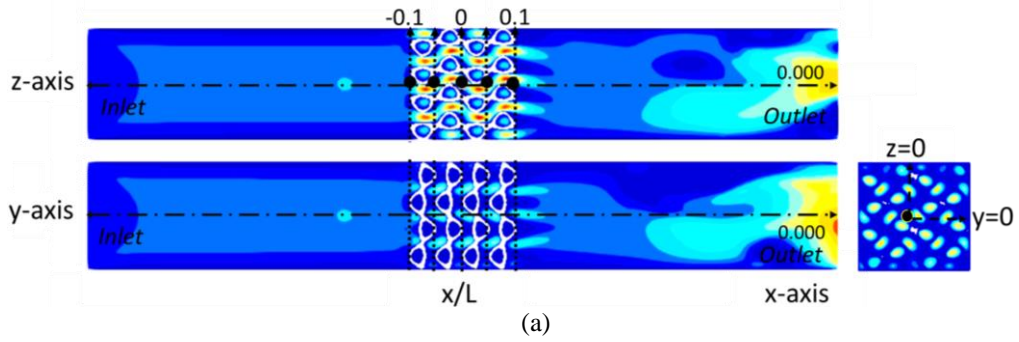


Fig. 6. Analysis of velocity profiles within TPMS split P lattice structures (a) data collection points on the yz plane, and (b) velocity of U_x/U_{ref} at point at $y = 0$ and $z = 0$ of SP0.4, SP0.8, and SP1.2 for various Reynolds numbers.

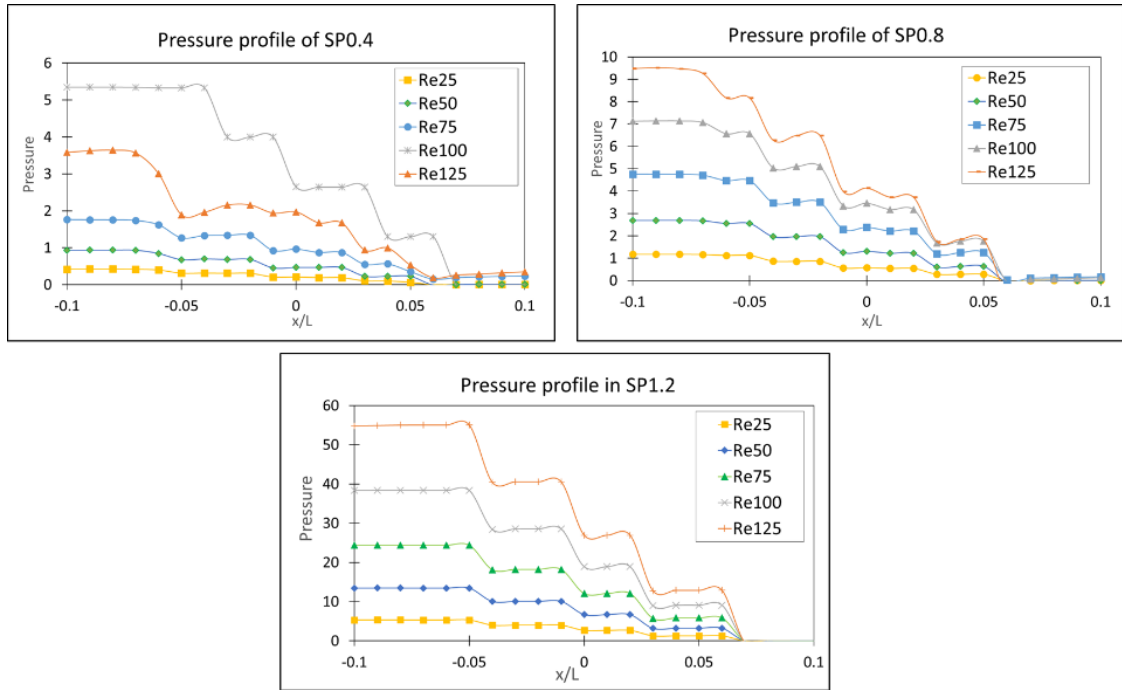


Fig. 7. Pressure profile at $z = 0, y = 0$ of SP0.4, SP0.8, and SP1.2 for various Reynolds numbers.

Pressure Profile Analysis

In a lattice structure, sudden changes in cross-sectional area are the cause of significant pressure variations between the inlet and outlet (Attarzadeh et al., 2022; Lee et al., 2022). Pressure reduction analysis clearly shows the effect of wall thickness on the changes in fluid pressure (see Fig 8).

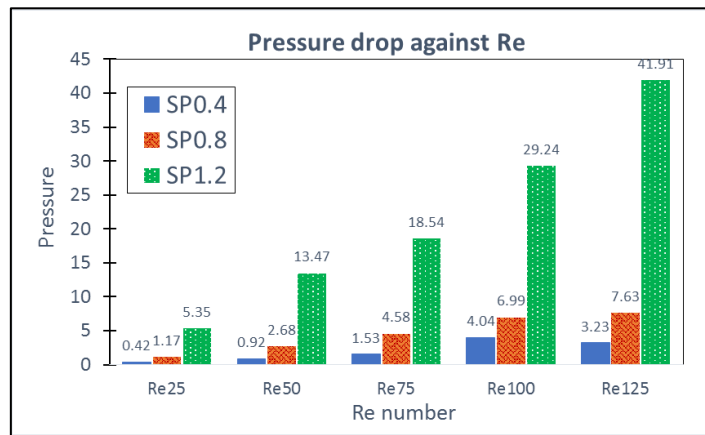


Fig. 8. Comparative pressure drops of TPMS split P lattice structures (SP0.4, SP0.8, and SP1.2) at various Reynolds numbers.

Increased wall thickness reduces pore size, resulting in greater resistance to flow as the fluid must navigate through a constricted space. The SP1.2 has the highest value of pressure loss, which is 9 times higher than SP0.4. For DAC application, local fluid pressure on the cell surfaces is an important parameter. Sufficient pressure must be exerted by the fluid on the adsorption catalyst in order to facilitate the carbon adsorption process. The 0.8 mm wall thickness obtained an ideal balance between pressure drop and velocity distribution, ensuring a more uniform and efficient flow through the lattice structure. Compared to earlier TPMS studies (Hawken et al., 2023; Zimmer et al., 2021) which focused primarily on gyroid and diamond structures, the split P lattice demonstrates superior flow uniformity and pressure reduction, crucial for optimizing DAC reactor performance. Therefore, a suitable split P lattice structure should be able to provide the required balance between high fluid-surface interaction (dependent on fluid velocity and distribution) with acceptable pressure reduction across the cell.

CONCLUSIONS

In this current study, the TPMS split P lattice with various thicknesses of the unit cell was examined under different inlet Reynolds numbers. The conclusions are as follows:

- i. Surface area and porosity: Reducing the wall thickness of the unit cell from 1.2 mm to 0.8 mm and 0.4 mm increased the total surface area by 1% to 4% and porosity from 12% to 23%, respectively. This optimization is significant for DAC systems, as it enhances the contact between air and the sorbent material, thereby improving CO₂ adsorption efficiency.
- ii. Fluid flow in split P: The smaller wall thickness significantly influences fluid flow within the split P structure, as demonstrated by a 128% increase in average fluid velocity. Furthermore, it allows for higher fluid velocity through the structure due to reduced flow resistance. This highlights the critical role of wall thickness in optimizing fluid flow, which is essential for ensuring efficiency and performance.
- iii. Pressure drops: The smaller pores, resulting from higher wall thickness, created greater resistance in the structure, leading to a lower average velocity for a given pressure difference. This occurs because friction and viscous forces limit the amount of fluid that can pass through. In relation to the split P design configuration for improved CO₂ capture, it is essential to find the right balance between pore size and flow efficiency to maximize surface area for effective performance.
- iv. Velocity distribution: Higher wall thickness caused the fluid to accelerate in confined spaces. This creates higher local velocities within the smaller pores as seen in SP1.2. This is why SP1.2 leads to a steeper velocity gradient, creating more significant velocity variations across the pores compared to SP0.8 and SP0.4. This causes higher maximum localized velocities compared to structures with larger pores.

Thus, given that lower averaged velocities could affect the efficiency of the absorption and desorption cycles, an optimal cell thickness between 0.4 mm and 0.8 mm is recommended. This balance ensures efficient mass transfer while minimizing excessive head loss. The numerical analysis successfully correlates the fluid flow within a split P lattice structure, and the simulation model allows further design optimization for an applied DAC system. Future work should focus on experimental validation of these CFD results, as well as the adaptation of the split P lattice for turbulent flow conditions to expand its applicability to higher Reynolds number regimes.

ACKNOWLEDGEMENT

We express our gratitude to the Research Management Center of Universiti Teknologi MARA for supporting this research through the Geran Insentif Penyelidikan (GIP) [600-RMC/GIP 5/3(123/2023)]. We also acknowledge the contributions of the Smart Manufacturing Research Institute (SMRI) and the School of Mechanical Engineering of Universiti Teknologi MARA for their support and facilities provided for this project. Our deepest appreciation goes to nTopology Inc. for its continuous support in providing advanced engineering design software, nTop, for this project.

CONFLICT OF INTERESTS

All authors declare that they have no conflicts of interest.

CONTRIBUTIONS OF AUTHORS

The authors confirm equal contribution in each part of this work. All authors reviewed and approved the final version of this work.

REFERENCES

- Alix, P., Roesler, J., Courtial, X., & Schultes, M. (2019). Hydraulic and mass transfer performances of a commercial hybrid packing: The RSP200X - Key modelling parameters for gas treatment applications. *Chemical Engineering Research and Design*, 147, 597–602.
- Al-Ketan, O., Ali, M., Khalil, M., Rowshan, R., Khan, K. A., & Al-Rub, R. K. A. (2020). Forced convection computational fluid dynamics analysis of architected and three-dimensional printable heat sinks based on triply periodic minimal surfaces. *Journal of Thermal Science and Engineering Application*, 13(2), 021010.
- Attarzadeh, R., Attarzadeh-Niaki, S. H., & Duwig, C. (2022). Multi-objective optimization of TPMS-based heat exchangers for low-temperature waste heat recovery. *Applied Thermal Engineering*, 212, 118448.
- Attarzadeh, R., Rovira, M., & Duwig, C. (2021). Design analysis of the “Schwartz D” based heat exchanger: A numerical study. *International Journal of Heat and Mass Transfer*, 177, 121415.
- Baghapour, B., Rouhani, M., Sharafian, A., Kalhori, S. B., & Bahrami, M. (2018). A pressure drop study for packed bed adsorption thermal energy storage. *Applied Thermal Engineering*, 138, 731–739.
- Bragin, D., Karpilov, I., & Pashchenko, D. (2024). Flow dynamics through cellular material based on a structure with triply periodic minimal surface. *Chemical Engineering Science*, 298, 120291.
- Chen, W., Tang, X., Chu, X., Yang, Y., Xu, W., Fu, D., Li, X., & Zhou, W. (2024). Impact of catalyst carrier with TPMS structures on hydrogen production by methanol reforming. *International Journal of Hydrogen Energy*, 58, 1177–1189.
- D’Orazio, A., Karimipour, A., & Ranjbarzadeh, R. (2023). Lattice Boltzmann modelling of fluid flow through porous media: A comparison between pore-structure and representative elementary volume

<https://doi.org/10.24191/jmeche.v22i2.3709>

- methods. *Energies*, 16(14), 5354.
- Dhoke, C., Zaabout, A., Cloete, S., & Amini, S. (2021). Review on reactor configurations for adsorption-based CO₂ capture. *Industrial and Engineering Chemistry Research*, 60(10), 3779–3798.
- Ellebracht, N. C., Roy, P., Moore, T., Gongora, A. E., Oyarzun, D. I., Stolaroff, J. K., & Nguyen, D. T. (2023). 3D printed triply periodic minimal surfaces as advanced structured packings for solvent-based CO₂ capture. *Energy and Environmental Science*, 16, 1752–1762.
- Gado, M. G., Ookawara, S., & Hassan, H. (2023). Utilization of triply periodic minimal surfaces for performance enhancement of adsorption cooling systems: Computational fluid dynamics analysis. *Energy Conversion and Management*, 277, 116657.
- Gunawardene, O. H. P., Gunathilake, C. A., Vikrant, K., & Amaraweera, S. M. (2022). Carbon dioxide capture through physical and chemical adsorption using porous carbon materials: A review. *Atmosphere*, 13(3), 397
- Hawken, M. B., Reid, S., Clarke, D. A., Watson, M., Fee, C. J., & Holland, D. J. (2023). Characterization of pressure drop through Schwarz-Diamond triply periodic minimal surface porous media. *Chemical Engineering Science*, 280, 119039.
- Jiang, L., Liu, W., Wang, R. Q., Gonzalez-Diaz, A., Rojas-Michaga, M. F., Michailos, S., Pourkashanian, M., Zhang, X. J., & Font-Palma, C. (2023). Sorption direct air capture with CO₂ utilization. *Progress in Energy and Combustion Science*, 95, 101069
- Karaman, D., & Asl, H. G. (2023). The effects of sheet and network solid structures of similar TPMS scaffold architectures on permeability, wall shear stress, and velocity: A CFD analysis. *Medical Engineering and Physics*, 118, 104024
- Kawalkar, R., Dubey, H. K., & Lokhande, S. P. (2022). A review for advancements in standardization for additive manufacturing. *Materials Today: Proceedings*, 50, 1983–1990.
- Laskowska, D., Szatkiewicz, T., Bałasz, B., & Mitura, K. (2023). Mechanical properties and energy absorption abilities of diamond TPMS cylindrical structures fabricated by selective laser melting with 316L stainless steel. *Materials*, 16(8), 3196.
- Lee, J. W., Oh, S. H., Jeon, E., Kim, J., & Park, K. (2022). Functional gradation of the morphological properties of TPMS channel for enhanced flow performance. *Materials and Design*, 224, 111413.
- Lehder, E. F., Ashcroft, I. A., Wildman, R. D., Ruiz-Cantu, L. A., & Maskery, I. (2021). A multiscale optimisation method for bone growth scaffolds based on triply periodic minimal surfaces. *Biomechanics and Modeling in Mechanobiology*, 20, 2085–2096.
- Li, L., & Iskander, M. (2022). Visualization of interstitial pore fluid flow. *Journal of Imaging*, 8(2), 32.
- Maconachie, T., Leary, M., Lozanovski, B., Zhang, X., Qian, M., Faruque, O., & Brandt, M. (2019). SLM lattice structures: Properties, performance, applications and challenges. *Materials and Design*, 183, 108137.
- Maskery, I., Aremu, A. O., Parry, L., Wildman, R. D., Tuck, C. J., & Ashcroft, I. A. (2018). Effective design and simulation of surface-based lattice structures featuring volume fraction and cell type grading. *Materials and Design*, 155, 220–232.

- Miralbes, R., Ranz, D., Pascual, F. J., Zouzias, D., & Maza, M. (2022). Characterization of additively manufactured triply periodic minimal surface structures under compressive loading. *Mechanics of Advanced Materials and Structures*, 29(13), 1841–1855.
- Nagarajan, B., Hu, Z., Song, X., Zhai, W., & Wei, J. (2019). Development of micro selective laser melting: The state of the art and future perspectives. *Engineering*, 5(4), 702–720.
- Patil, T., Dharaskar, S., Sinha, M., & Jampa, S. S. (2022). Effectiveness of ionic liquid-supported membranes for carbon dioxide capture: a review. *Environmental Science and Pollution Research*, 29, 35723–35745.
- Peng, H., Gao, F., & Hu, W. (2020). Design, modeling and characterization of triply periodic minimal surface heat exchangers with additive manufacturing. *Proceeding of the 30th Annual International Solid Freeform Fabrication Symposium (pp. 2325–2337)*. University of Texas.
- Plocher, J., & Panesar, A. (2019). Review on design and structural optimisation in additive manufacturing: Towards next-generation lightweight structures. *Materials and Design*, 183, 108164. <https://doi.org/10.1016/j.matdes.2019.108164>
- Rabuan, N., Adenan, M. S., Manurung, Y. H. P., Anuar, M. A. M., & Shuib, S. (2023). Structural performance of Ti6Al4V tibial tray in total knee arthroplasty (TKA) by functionally graded lattice structures using numerical analysis. *Journal of Mechanical Engineering*, 12, 153–172. <https://doi.org/10.24191/JMECHE.V12I1.24643>
- Tang, W., Zhou, H., Zeng, Y., Yan, M., Jiang, C., Yang, P., Li, Q., Li, Z., Fu, J., Huang, Y., & Zhao, Y. (2023). Analysis on the convective heat transfer process and performance evaluation of triply periodic minimal surface (TPMS) based on Diamond, Gyroid and Iwp. *International Journal of Heat and Mass Transfer*, 201(1), 123642.
- Wood, B. D., He, X., & Apte, S. V. (2020). Modeling turbulent flows in porous media. *Annual Review of Fluid Mechanics*, 52, 171–203.
- Xu, H., Yu, W., Zhang, Y., Ma, S., Wu, Z., & Liu, X. (2023). Flow and heat transfer performance of bionic heat transfer structures with hybrid triply periodic minimal surfaces. *Applied Energy*, 351, 121847.
- Xu, W., Yu, A., Lu, X., Tamaddon, M., Wang, M., Zhang, J., Zhang, J., Qu, X., Liu, C., & Su, B. (2021). Design and performance evaluation of additively manufactured composite lattice structures of commercially pure Ti (CP-Ti). *Bioactive Materials*, 6(5), 1215–1222.
- Xu, Y., Han, G., Huang, G., Li, T., Xia, J., & Guo, D. (2023). Properties evaluations of topology optimized functionally graded lattice structures fabricated by selective laser melting. *Materials*, 16(4), 1700.
- Young, J., Mcilwaine, F., Smit, B., Garcia, S., & Spek, M. V. D. (2023). Process-informed adsorbent design guidelines for direct air capture. *Chemical Engineering Journal*, 456, 141035.
- Yin, X., Meng, W., Cheng, J., Wang, H., & Zhao, X. (2021). A kind of filling lattice structure based on DFAM for mechanical parts: The diamond lattice structure. *Advances in Materials Science and Engineering*, 2021(1), 8816593.
- Yu, Q., & Brilman, D. W. F. (2017). Design strategy for CO₂ adsorption from ambient air using a supported amine based sorbent in a fixed bed reactor. *Energy Procedia*, 114, 6102–6114.
- Zhang, L., Hu, Z., Wang, M. Y., & Feih, S. (2021). Hierarchical sheet triply periodic minimal surface <https://doi.org/10.24191/jmeche.v22i2.3709>

lattices: Design, geometric and mechanical performance. *Materials & Design*, 209, 109931.

Zimmer, A., PachecoAraújo, J. D., Andreassen, K. A., & Grande, C. A. (2021). Effect of manufacturing techniques in pressure drop on triple periodical minimal surface packings. *Chemie Ingenieur Technik*, 93(6), 967–973.